Materials Transactions, Vol. 65, No. 11 (2024) pp. 1397 to 1401

Production of Solidified Body from a Melt and Its Electrical Conductivity of $CsSnBr_3$ Using Precursor Prepared by Mechanochemical Reaction Process*1

Kiyoshi Kobayashi*2, Shogo Miyoshi and Tohru S. Suzuki

National Institute for Materials Science, Tsukuba 305-0047, Japan

Cesium-tin-bromide perovskite ($CsSnBr_3$) has focused on as a candidate material for all-inorganic perovskite solar cell and thermoelectric energy converter because of its optical, electrical, and thermal properties. On the other hand, the electrical properties have not been clarified yet because of several inconsistent reports. In this paper, we produced $CsSnBr_3$ bulk from a melt using the precursor powder prepared by a mechanochemical process. From powder X-ray diffraction analysis, main phase of the precursor was $CsSnBr_3$ perovskite, and minor impurities were Cs_2SnBr_4 and $CsSn_2Br_5$. Although main phase of the bulk produced from a melt was $CsSnBr_3$, small amount impurity, $CsSn_2Br_5$ was confirmed. From the electrical conductivity (σ_t) measurement, irreversible temperature dependence of σ_t was observed at first time increasing temperature. The conductivity measured from room temperature to 443 K at the first time showed metallic behavior. On the other hand, the temperature dependence is changed into opposite with decreasing temperature. At this operation, σ_t decrease with decreasing temperature. This semiconductor like behavior was found to be reversible after first increasing temperature operation. These results indicate that post anneal as well as production process of $CsSnBr_3$ would be important to control its electric property. [doi:10.2320/matertrans.MT-Y2024005]

(Received June 11, 2024; Accepted August 19, 2024; Published October 25, 2024)

Keywords: *$CsSnBr_3$, cesium tin bromide, perovskite, mechanochemical synthesis, electrical conductivity*

1. Introduction

The cubic cesium tin bromide perovskite ($CsSnBr_3$) is a potential material for all-inorganic perovskite solar cells and thermoelectric energy conversion materials because of its excellent optical, electrical, and thermal properties [1, 2]. Nevertheless, the synthesis difficulty was understood from the phase relationship in the CsBr-$SnBr_2$ system (Fig. 1) [3, 4]. Although the melting point of $CsSnBr_3$ is approximately 723 K, the eutectic point exists around 10 mol% CsBr-90 mol% $SnBr_2$ at 477 K. Therefore, when a mixed powder with 50 mol% CsBr-50 mol% $SnBr_2$ is heated directly, a liquid with a composition around 10 mol% CsBr-90 mol% $SnBr_2$ is initially formed at 477 K; then, the liquid is precipitates at the bottom of the container. The precipitation of the liquid around the 10 mol% CsBr-90 mol% $SnBr_2$ composition continues on further heating. As the results, even though the mixed powder is changed into liquid above 723 K, it is difficult to obtain a homogeneous liquid. Therefore, in order to obtain the homogeneous $CsSnBr_3$ solidified body from the melt, it is necessary to use a special instrument for stirring the liquid above 723 K.

In oxide systems with similar phase relationship to the CsBr-$SnBr_2$ system, the inhomogeneity can be prevented by employing low-temperature synthesis processes, such as coprecipitation and sol-gel methods [5–8]. However, the wet process using solvent-like coprecipitation and sol-gel methods is difficult to apply to a non-oxide system. A notable dry process suitable for low-temperature synthesis is the mechanochemical method. In the mechanochemical method, the driving force of chemical reactions is impact force; therefore, heating is unnecessary. Hence, the liquid formation at the eutectic point, as shown in Fig. 1, and the precipitation of the liquid do not occur. Thus, a homogeneous liquid with a $CsSnBr_3$ composition can be prepared.

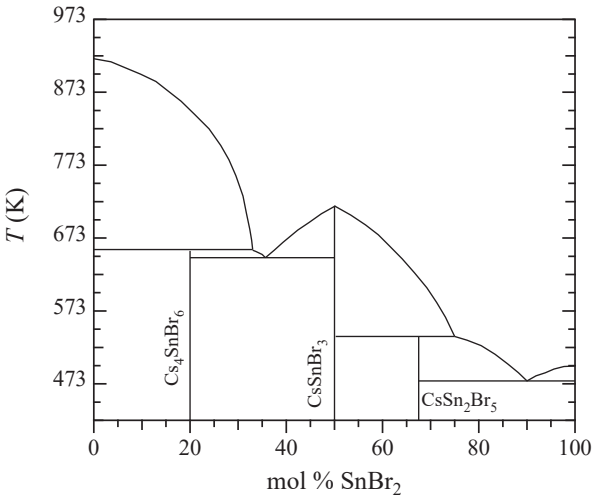

Fig. 1 Phase diagram in CsBr-$SnBr_2$ system [3, 4].

Although the $CsSnBr_3$ perovskite is expected to be a suitable material for all-solid perovskite solar cells and thermoelectric devices, its electrical property is not clarified yet. Only a few studies have reported on the electrical conductivity (σ_t) of the $CsSnBr_3$ bulk. Moreover, the temperature dependence of σ_t shows large discrepancy among different reports [2, 9–11]; certain studies conclude that the temperature dependence of σ_t exhibits a metal-like behavior, whereas others report that σ_t shows semiconductor-like behavior.

In this study, we employed a mechanochemical reaction process to prepare a precursor for producing the homogeneous $CsSnBr_3$ melt [12, 13]. Further, we produced the $CsSnBr_3$ bulk from the melt and investigated its electrical conductivity.

*1This Paper was Originally Published in Japanese in J. Japan Soc. Powder Powder Metallurgy **70** (2023) 427–431.

*2Corresponding author, E-mail: kobayashi.kiyoshi@nims.go.jp

2. Experiments

2.1 Mechanochemical synthesis

Cesium bromide (CsBr, 99.9%, Wako Pure Chemical Industries, Ltd., Japan) and tin (II) bromide anhydrous ($SnBr_2$, 99.9%, Kojundo Chemical Lab. Ltd., Japan) were used as raw materials. In a nitrogen-filled glove box, the same molar amount of CsBr and $SnBr_2$ were weighed to a total amount of 20 g. The weighed CsBr and $SnBr_2$ were set in a calcia-stabilized zirconia (CSZ) pot. Then, approximately 100 g of yttria-stabilized zirconia (YSZ) balls were set in the CSZ pot. The diameter of the ball was 10 mm. A cap with a Teflon® ring was put on the pot. Subsequently, the pot and cap set was placed in an enclosed stainless steel container. The container was taken out from the glove box and set in a planetary ball mill instrument (PULVERETTE 6, Fritsche, German). The mechanochemical reaction was conducted at 400 rpm for 3 h. After the milling, the mechanochemically reacted sample was scraped off from the inside wall of the pot in the glove box. The scraped sample and YSZ balls were placed in the pot and placed in the enclosed stainless-steel container. The sample was mechanochemically reacted again under the same conditions as the first time. The reacted sample was scraped off from the pot and pulverized into powder using a zirconia mortar and pestle in the glove box, and the powder was used as a precursor to produce the solidified body from the melt. The formed phase of the precursor was confirmed by using X-ray diffraction (XRD) instrument (TTR-III, Rigaku Co. Ltd., Japan).

2.2 Production of solidified body from the melt

The precursor powder was enclosed in a vacuum quartz glass tube of diameter 10 mm. The glass tube was heated at 823 K in a vertically placed electric furnace. It was gradually cooled by moving it down from the center to the bottom of the furnace. The moving rate was 0.01 mm/s. Hence, the solidified body with a diameter of approximately 10 mm and a length of 60 mm was obtained. The solidified body was removed from the quartz tube at room temperature; then, a disk shape sample of 1.7 mm thickness was cut from the body using a low-speed diamond blade saw. Herein, the disk is denoted as a solidified disk. The formed phase at the surface of the cut disk was confirmed by XRD analysis.

A part of the solidified body was fractured to conduct composition analysis using an energy dispersive X-ray spectrum meter (Element EDS, EDAX, USA). The spectrum meter was attached to a scanning electron microscope (FlexSEM 1000 II, Hitachi High-Tech. Corp., Japan).

To confirm the validity of the precursor, a solidified body from a melt was produced using a CsBr-$SnBr_2$ mixed powder. The production condition was the same to the body made from the precursor powder. The formed phase was analyzed by the XRD pattern from the cut surface similar to the surface prepared from the disk surface made from the precursor powder.

2.3 Electrical conductivity measurement

Carbon disks were used as electrodes. The solidified disk was sandwiched by two carbon disks. Platinum wires were wound around each carbon disk as lead wires. The conductivity was measured under nitrogen flow in the temperature range between room temperature and 448 K. The measurements were carried out while repeatedly increasing and decreasing the temperature cycle between the room temperature and 448 K. Electrical conductivity measurements were carried out based on the two-probe impedance method using a potentiostat/galvanostat (Reference 600, Gamry, USA). No clear spectra were observed by impedance measurements due to the relaxation process; therefore, the spectra were explained only by the resistor. The total conductivity was calculated from the resistance, surface area, and thickness of the solidified disk.

3. Results and Discussions

3.1 Mechanochemical reaction

Macroscopic pictures of the 50 mol% CsBr-50 mol% $SnBr_2$ mixed powder and the precursor obtained by the mechanochemical reaction are shown in Fig. 2. The raw material mixture (50 mol% CsBr-50 mol% $SnBr_2$) is white because CsBr and $SnBr_2$ are colorless. Conversely, the precursor is black; therefore, the chemical reaction is visually found to proceed by the impact force at planetary ball milling. The main peak positions in the XRD pattern collected from the precursor powder is found to show good agreement with the peak positions of $CsSnBr_3$ [14] (Fig. 3). The positions of other small peaks showed good agreement with those of Cs_4SnBr_6 and $CsSn_2Br_5$ [3, 15]. These formed phases are compounds having lower $SnBr_2$ composition compared to the eutectic one (90 mol% $SnBr_2$) shown in Fig. 1. It was found that formation of the inhomogeneous liquid at 477 K due to the eutectic reaction as shown in Fig. 1 was prevented by the mechanochemical reaction even though the mechanochemical reaction was essentially a solid-state reaction process.

3.2 Solidified body from a melt

The XRD pattern collected from the cut surface of the

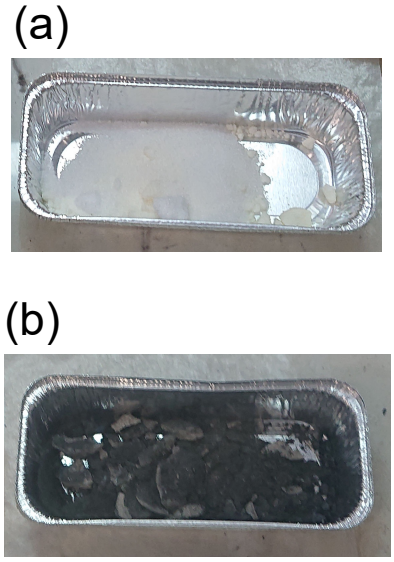

Fig. 2 Overview of (a) mixed powder of raw materials, CsBr and $SnBr_2$, and (b) precursor obtained by mechanochemical reaction.

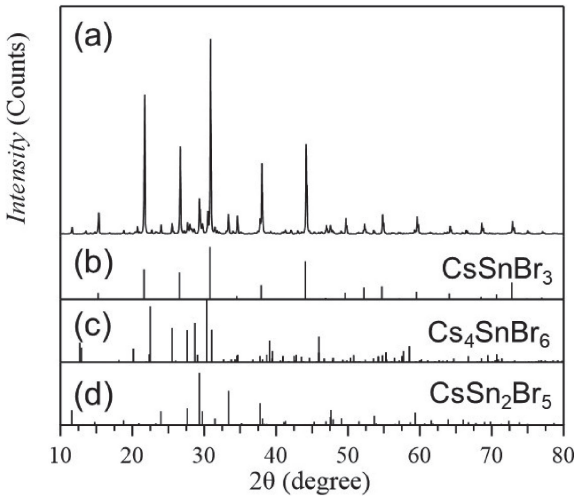

Fig. 3 X-ray diffraction pattern of (a) the precursor obtained by mechanochemical reaction. Calculated patterns of (b) $CsSnBr_3$ [14], (c) Cs_4SnBr_6 [3], and (d) $CsSn_2Br_5$ [15] are plotted for comparison.

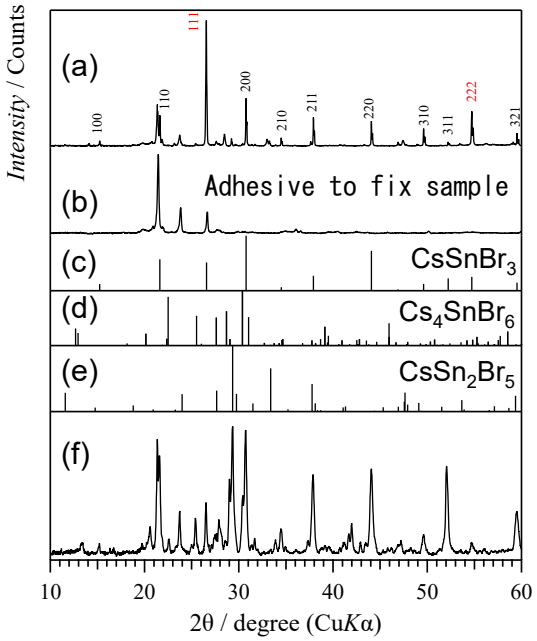

Fig. 4 (a) X-ray diffraction pattern collected from a cut surface of $CsSnBr_3$ solidified body from a melt using a precursor by mechanochemical reaction. X-ray diffraction patterns of (b) adhesive used to fix the sample, and calculated patterns of (c) $CsSnBr_3$ [14], (d) Cs_4SnBr_6 [3], and (e) $CsSn_2Br_6$ [15] are plotted for comparison. X-ray diffraction pattern collected from a cut surface $CsSnBr_3$ solidified body prepared from 50 mol% CsBr-50 mol% $SnBr_2$ mixture.

solidified body from the melt is shown in Fig. 4(a). Except for the XRD pattern of an adhesive to fix the solidified disk (Fig. 4(b)), the main peaks were found to show good agreement with $CsSnBr_3$ peaks. On comparing the peaks between the precursor powder and the cut surface of the solidified disk, the $CsSn_2Br_5$ peak intensities were relatively low. In addition, the peaks of Cs_4SnBr_6 were not present in the solidified disk. Based on these results, the amount of impurity segregation decreased in the case of the solidified disk.

After comparing the reported XRD peaks of $CsSnBr_3$, the peak intensities at 111 and 222 that were collected from the

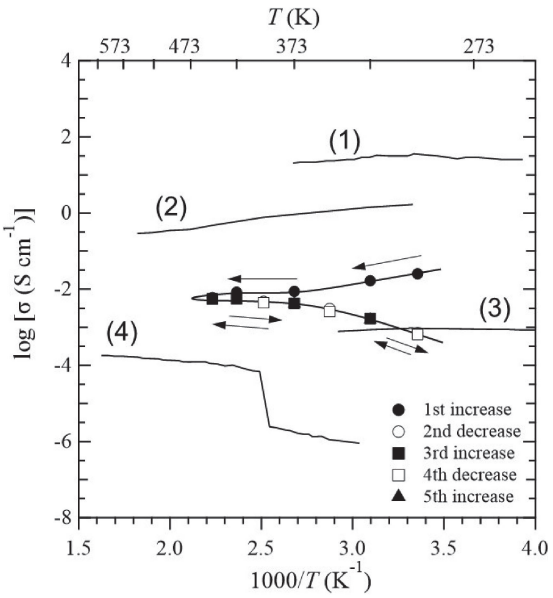

Fig. 5 Arrhenius plot of $CsSnBr_3$ solidified body using mechanochemical precursor. Conductivity data from (1) Ref. [10], (2) Ref. [2], (3) Ref. [9], and (4) Ref. [11] are plotted for comparison.

solidified disk surface were relatively high. Therefore, the cut surface of the solidified disk was oriented to the [111] direction in which large grains existed. In this study, the solidified body was produced by slow cooling from the melt of the precursor enclosed in a vacuum quartz glass tube. From this method, single crystal and/or large grains were preferably grown from seeds formed during slow cooling. Large grains oriented to the [111] direction were contained because a tendency of the crystal orientation was observed by the XRD pattern.

The XRD pattern collected from the cut surface of the solidified body produced from the 50 mol% CsBr-50 mol% $SnBr_2$ powder is shown in Fig. 4(f). From this pattern, no peaks from $CsSnBr_3$ were confirmed; further, phase identification was not possible. The reason for the formation of such solidified bodies was suggested to be the lack of homogeneity of the liquid composition as explained in the introduction.

3.3 Electrical conductivity

Figure 5 shows an Arrhenius plot of σ_t measured using the solidified disk. At the first increase of the temperature process from room temperature to 448 K, σ_t decreased with an increasing temperature, i.e., metal-like behavior. Then, the temperature dependence of σ_t was changed to a semiconductor-like behavior when σ_t decreased with a decreasing temperature. Subsequently, σ_t showed a reversible temperature dependency by repeating the temperature cycle as shown in Fig. 5, i.e., semiconductor-like behavior. The activation energy calculated from the slope of the Arrhenius plot was 0.02 eV above 333 K and 0.3 eV below 333 K. The critical temperature of 333 K is different from the reported one of the semimetal - semiconductor phase transition (393 K) [11] and structural phase transition (286 K) [14]. In addition, this our results are different from the reported one that the σ_t spike appeared at the semimetal - semiconductor

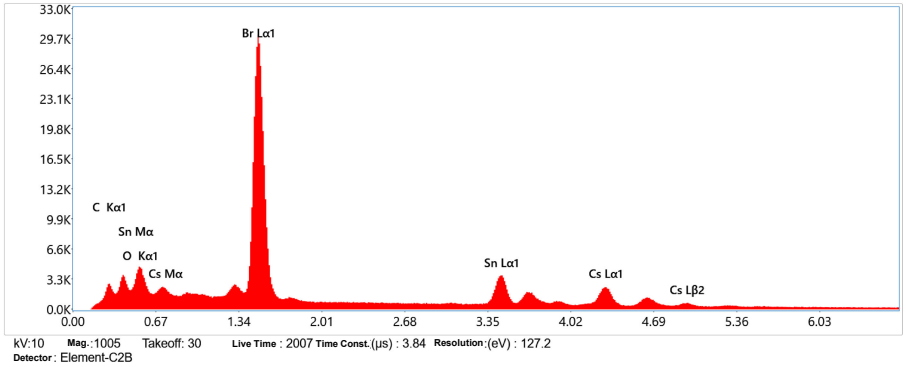

eZAF Quant Result - Analysis Uncertainty: 16.37 %			
Element	Weight%	Atom%	Error %
C K	9.17	41.73	12.63
O K	3.04	10.38	10.91
Br L	39.42	26.95	5.94
Sn L	21.31	9.81	5.66
Cs L	27.06	11.13	7.44

Fig. 6 Results of composition analysis on a fracture surface of $CsSnBr_3$ solidified body from a melt using mechanochemical precursor.

phase transition [11]. The origin of the activation energy change has not been clarified yet.

The reported $\log \sigma_t$ values shown in Fig. 5 show a wide scattering range from −2 to −6. The reported results on temperature dependence showed a large discrepancy because of the metal-like behavior [2, 9, 10], semiconductor-like behavior [11], and existence (or not) of $\log \sigma_t$ spike due to the phase transition. The $\log \sigma_t$ values obtained in this study fall in the range of the existing reported data [2, 9–11]. The $\log \sigma_t$ with semiconductor-like behavior was reversible for the temperature cycle. However, no $\log \sigma_t$ spike appeared.

The observed differences were attributed to variations in the sample production process. The sample showing a $\log \sigma_t$ spike due to the semimetal - semiconductor transition was a single crystal [11, 16] grown from heated ethylene glycol dissolved CsBr and $SnBr_2$. The single crystal was grown by slowly cooling the solution. The sample production process was different from our study. Regarding the conductivity measurement, σ_t of the single crystal was reported to be measured after several temperature cycles in order to appear reversible temperature dependence of σ_t to remove an influence on thermal stress and so on [11]. The fact that temperature dependence of σ_t became reversible after several temperature cycles was similar to our results.

The bulk and single crystal samples showing metal-like behavior is produced by slow cooling from a melt [2, 9, 10]. The melt was produced from a mixture of CsBr and $SnBr_2$. With regards to the temperature reversibility of σ_t, there was no explanation; therefore, the same phenomenon of the temperature behavior of σ_t observed at the first temperature increase of our sample possibly occurred.

The anisotropy of σ_t might not appear for $CsSnBr_3$ because of its cubic structure. Therefore, the difference between our σ_t results and the reported data is not due to the 111 crystal orientation as explained in Fig. 4.

Based on these results, $CsSnBr_3$ probably has several metastable states. The solidified bulk and single crystal are frozen at the metallic metastable state that may be transformed into a stable semiconductor phase by increasing the temperature. The stability of this semiconductor phase was high; therefore, the reversible temperature dependence on σ_t appeared after the first temperature increase.

The reason that reported σ_t values are scattered in approximately a 4-order range is probably a difference in impurity composition. From the chemical analysis from the fractured surface of the solidified rod used in this research, a negligible amount of oxygen was detected (Fig. 6). However, we could not be achieved a quantitative estimation because of the large error. When oxygen was substituted at the bromide ion site, a hole was formed due to the difference in their valence numbers. Further investigation is necessary to investigate the oxygen contamination observed because there has been no report on this so far. In addition, a defect chemical analysis involving the doping of aliovalent ions is also necessary because of the absence of studies on $CsSnBr_3$ that investigate its defect chemistry.

Another possible contaminant is zirconia because we employed the mechanochemical reaction using a zirconia pot and balls. The Zr-Lα peak should appear at 2.04 keV in the energy dispersive X-ray spectrum (EDS). By confirmation of Fig. 6, no peak is found at 2.04 keV; therefore, the concentration of Zr in our sample is lower than the detection limit of the spectrum meter (1 atom%). Hence, the contamination of Zr is ignorable.

The electric properties must be controlled for applications to perovskite solar cells and thermoelectric devices; in particular, the stability of electric properties is important. As explained above, not only the absolute value but also the temperature dependence of σ_t for $CsSnBr_3$ strongly depends on the production process. The temperature reversibility of σ_t results in stable electric properties. Hence, post annealing is necessary to produce $CsSnBr_3$ samples with stable electric properties.

4. Conclusion

In this study, a $CsSnBr_3$ precursor powder was prepared by the mechanochemical reaction to produce the solidified body from the melt. In addition, the solidified body was produced using the precursor; then, the electrical conductivity was measured using the solidified disk cut from the body.

The colorless mixed powder of CsBr and $SnBr_2$ was changed into a black powder by a mechanochemical reaction. Although the main phase of the blackened precursor was $CsSnBr_3$, small peaks from $CsSn_2Br_6$ were observed. From the XRD analysis of the solidified body produced from the 50 mol% CsBr-50 mol% $SnBr_2$ powder, the peaks from $CsSnBr_3$ were not observed and phase identification was not feasible because of the formation of inhomogeneous liquid. Therefore, we confirmed that the $CsSnBr_3$ precursor preparation process was valid for the production of the $CsSnBr_3$ solidified body from the melt.

The total electrical conductivity (σ_t) measured at the first temperature increase showed metallic behavior, i.e., σ_t decreased as the temperature increased. On the contrary, σ_t changed into a semiconductor-like behavior because σ_t decreased as the temperature decreased in the temperature range from 448 K to room temperature. Thus, the σ_t values were different when σ_t was measured at the first temperature increase and the subsequent temperature decline. After the first temperature cycle, σ_t demonstrated a reversible temperature change with a semiconductor-like behavior. Based on these results, we concluded that the produced $CsSnBr_3$ solidified bulk was in a metastable state. The Arrhenius plot of the reversible σ_t showed a bend at 333 K, which was in disagreement with the reported phase transition temperatures. Moreover, a large variation of σ_t values of $CsSnBr_3$ has been confirmed in previous studies. Thus, further research is necessary to clarify the electrical properties of $CsSnBr_3$.

Acknowledgments

This work was supported by the JSPS KAKENHI Grant Number 17H01317.

REFERENCES

[1] M. Roknuzzaman, K. Ostrikov, H. Wang, A. Du and T. Tesfamichael: Towards lead-free perovskite photovoltaics and optoelectronics by ab-initio simulations, Sci. Rep. **7** (2017) 14025.

[2] H. Xie, S. Hao, J. Bao, T.J. Slade, G.J. Snyder, C. Wolverton and M.G. Kanatzidis: All-inorganic halide perovskites as potential thermoelectric materials: Dynamic cation off-centering induces ultralow thermal conductivity, J. Am. Chem. Soc. **142** (2020) 9553–9563.

[3] B.M. Benin, D.N. Dirin, V. Morad, M. Wörle, S. Yakunin, G. Rainó, O. Nazarenko, M. Fischer, I. Infante and M.V. Kovalenko: Highly emissive self-trapped excitons in fully inorganic zero-dimensional tin halides, Angew. Chem. Int. Ed. **57** (2018) 11329–11333.

[4] R.H. Andrews, S.J. Clark, J.D. Donaldson, J.C. Dewan and J. Silver: Solid-state properties of materials of the type-Cs_4MX_6 (where M = Sn or Pb and X = Cl or Br), J. Phys. Chem. Dalton Trans. (1983) 767–770.

[5] S. Kitajima, K. Kobayashi, T. Higuchi and Y. Sakka: Development of new synthesis route of lanthanum germanate oxyapatite from homogeneous aqueous solution, Ceram. Trans. **243** (2014) 103–108.

[6] Y. Igarashi, S. Kitajima, K. Kobayashi, T. Higuchi and Y. Sakka: Low-temperature synthesis process of lanthanum germanate oxyapatite by citrate combustion method, J. Jpn. Soc. Powder Powder Metallurgy **61** (2014) 582–586.

[7] K. Kobayashi, S. Kitajima, Y. Igarashi, T. Higuchi and Y. Sakka: Research and development of the coprecipitation process for lanthanum germanate oxyapatite, J. Am. Ceram. Soc. **98** (2015) 66–70.

[8] K. Kobayashi, Y. Igarashi, N. Saito, T. Higuchi, T. Sakka and T.S. Suzuki: Stabilization of the high-temperature phase and total conductivity of yttrium-doped lanthanum germanate oxyapatite, J. Ceram. Soc. Jpn. **126** (2018) 91–98.

[9] S. Clark, C.D. Flint and J.D. Donaldson: Luminescence and electrical conductivity of $CsSnBr_3$ and related phases, J. Phys. Chem. Solids **42** (1981) 133–135.

[10] K. Yamada, H. Kawaguchi, T. Matsui, T. Okuda and S. Ichiba: Structural phase-transition and electrical-conductivity of the perovskite $CH_3NH_3Sn_{1-x}Pb_xBr_3$ and $CsSnBr_3$, Bull. Chem. Soc. Jpn. **63** (1990) 2521–2525.

[11] R.L. Narayan and S.V. Suryanarayana: Transport-properties of the perovskite-type halides, Mater. Lett. **11** (1991) 305–308.

[12] Z. Hong, D. Tan, R.A. John, T.D.E. Tay, Y.K.T. Ho, X. Zhao, Z.C. Sum, N. Mathews, F. Garcia and H.S. Soo: Completely solvent-free protocols to access phase-pure, metastable metal halide perovskites and functional photodetectors from the precursor salts, iScience **16** (2019) 312–325.

[13] Y.E. Ajjouri, F. Locardi, M.C. Gélvez-Rueda, M. Prato, M. Sessolo, M. Ferretti, F.C. Grozema, F. Palazon and H.J. Bolink: Mechanochemical synthesis of Sn(II) and Sn(IV) iodide perovskites and study of their structural, chemical, thermal, optical, and electrical properties, Energy Tech. **8** (2019) 1900788.

[14] D.H. Fabini, G. Laurita, J.S. Bechtel, C.C. Stoumpos, H.A. Evans, A.G. Kontos, Y.S. Raptis, P. Falaras, A. van der Ven, M.G. Kanatzidis and R. Seshadri: Dynamic stereochemical activity of the Sn^{2+} lone pair in perovskite $CsSnBr_3$, J. Am. Chem. Soc. **138** (2016) 11820–11832.

[15] D. Becker and H.P. Beck: High pressure study of $NH_4Pb_2Br_5$ type compounds. I Structural parameters and their evolution under high pressure, Z. Anorg. Allg. Chem. **630** (2004) 1924–1932.

[16] M. Mori and H. Saito: An X-ray study of successive phase-transition in $CsSnBr_3$, J. Phys. C **19** (1986) 2391–2401.